JOURNAL OF MATERIALS SCIENCE 33 (1998) 29–33

The effective tensile failure stress of an uncracked brittle structure: failure at a blunt stress concentration

E. SMITH
Manchester University – University of Manchester Institute of Science and Technology, Materials Science Centre, Grosvenor Street, Manchester M1 7HS, UK

The paper proceeds from the basis that the dominant source of the geometry dependence of the effective tensile failure stress of an uncracked brittle structure is deterministic and is related to the formation of a damage zone at a free surface. The damage is represented by a cohesive zone, and failure, i.e. the attainment of maximum load, is associated with the attainment of an elastically calculated effective tensile failure stress. With regard to failure arising as a result of the formation of a damage zone at the surface of a blunt stress concentration, the paper predicts the extent to which the effective tensile failure stress increases with increasing severity of the stress concentration, i.e. as the root radius decreases.

1. Introduction

It is a well-known experimental fact that the effective tensile failure stress of an uncracked brittle structure depends on its dimensions. This is best, and very simple, illustrated by considering the case of an uncracked bend beam specimen for which the maximum stress occurs at the tensile surface. Assuming elastic behaviour, if the beam depth is d and the beam thickness is B, the bending moment is equal to $Bd^2\sigma_s/6$, where σ_s is the tensile stress at the surface. Experiments [1, 2], for example with unreinforced concrete beams, have shown that the maximum moment M_m that a beam is able to sustain is equal to $Bd^2\sigma_s/6$ with $\sigma_s = \sigma_m$ and where σ_m (the effective tensile failure stress) increases as the beam depth d decreases.

As recently emphasized by Li and Bazant [3], the underlying cause of this geometry dependence for brittle and quasibrittle materials such as concrete, sea ice, rocks, tough ceramics and composites is associated with the experimental observation that they exhibit damage zones which are able to grow in a stable manner prior to the attainment of maximum load. That being the case, the dominant source of the geometry dependence is not randomness of strength, but rather it is deterministic and is related to the manner in which such a zone develops. From this basis, and in the context of the bend specimen geometry, the present author [4] has shown that the effective tensile failure stress is critically dependent on the applied loading-induced stress gradient beneath the surface of a structure. The effective tensile failure stress increases with increasing steepness of this gradient, and we therefore have a ready explanation as to why the effective tensile failure stress for an uncracked beam increases as the beam depth decreases.

The present paper builds on these earlier considerations by considering the formation of a damage zone at the surface of a blunt stress concentration, instead of a planar surface, and the results of a theoretical analysis demonstrate the extent to which the effective tensile failure stress increases with increasing severity of the stress concentration, i.e. as the root radius decreases.

2. Outline of the cohesive zone description of a damage zone

The simplest way of representing a damage zone is to use the so-called cohesive zone description, whereby a single, infinitesimally thin two-dimensional cohesive zone starts to form at the surface of a structure when the tensile stress at the surface attains some critical value p_c (we are assuming plane-strain deformation conditions). As the applied load (stress) increases, the zone spreads away from the surface into the interior of the structure. The zone can be characterized by a material-specific relation between the tensile stress, p, and the relative displacement, v, between the zone faces, with p being a maximum, p_c, at the leading edge of the cohesive zone. The zone is said to be fully developed when the stress falls to zero at the trailing edge of the zone, i.e. at the surface, a situation that is assumed to be attained when the displacement v attains a critical value, v_c. With a general p–v cohesive zone behaviour, the maximum load (stress), and thereby failure, is attained prior to the cohesive zone's full development. However, so as to simplify the considerations, it will, in this paper, be assumed that the stress, p, within the cohesive zone remains constant at the value p_c until the displacement, v, attains the critical value, v_c, when

0022–2461

the stress, p, is assumed to fall abruptly from p_c to zero. This is the classic Dugdale–Bilby–Cottrell–Swinden (DBCS) [5, 6] representation that is frequently used to model stress relaxation phenomena. With this specific cohesive zone behaviour, the attainment of maximum load (stress), and thereby failure, is associated with the full development of the cohesive zone.

3. Cohesive zone formation at a cylindrical hole: use of mode III simulation model results

Consider the situation where there is a two-dimensional elliptically cylindrical hole in an infinite solid (Fig. 1), which is subjected to the applied tensile stress, σ. The semimajor axis is a and the semiminor axis is b, whereupon the radius of curvature at the ends of the major axis is $\rho = b^2/a$. Cohesive zones of the type described in the preceding section emanate from the roots of the hole as shown in Fig. 1.

The antiplane strain (mode III) analogue of the plane-strain (mode I) model in Fig. 1 can be analysed to give closed-form solutions, thereby enabling one to have a clear picture of the way in which the various geometrical and material parameters interact. Thus the mode III results [7] will be used for the mode I situation with the shear modulus being replaced by $E_0/2$, where E_0 is the reduced Young's modulus of the material, i.e. $E_0 = E/(1-\nu^2)$, E being Young's modulus and ν being Poisson's ratio. The results give the maximum stress required for failure, i.e. for the relative displacement at a flaw root to attain a critical value, v_c, as

$$\frac{\sigma}{p_c} = \frac{b/a}{1+b/a} + \frac{2}{\pi(1+b/a)} \sec^{-1}\left[\exp\left(\frac{\pi E_0 v_c}{8 p_c a}\right)\right] \quad (1)$$

If the effective failure stress, i.e. the elastically calculated stress, is σ_{eff}, i.e.

$$\frac{\sigma_{eff}}{\sigma} = 1 + \frac{a}{b} \quad (2)$$

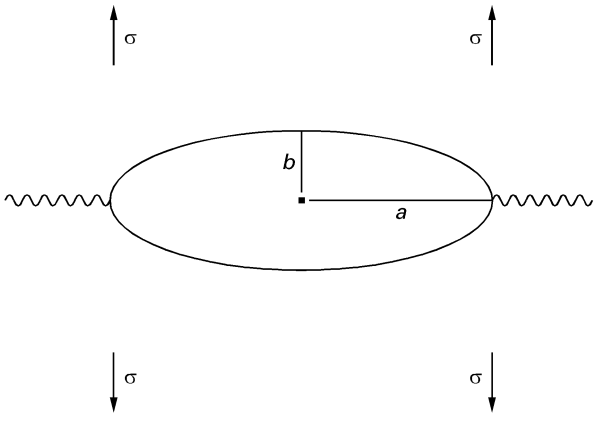

Figure 1 The model of an elliptically cylindrical hole in an infinite solid subjected to an applied tensile stress σ; there are cohesive zones at the roots of the hole.

it follows from Equations 1 and 2 that

$$\frac{\sigma_{eff}}{p_c} = 1 + \frac{2}{\pi}\left(\frac{a}{\rho}\right)^{1/2} \sec^{-1}\left[\exp\left(\frac{\pi E_0 v_c}{8 p_c a}\right)\right] \quad (3)$$

Furthermore, the mode III analytical results give the cohesive zone size associated with the attainment of maximum stress as

$$\frac{s}{a} = (\chi - 1) + \left(\frac{\rho}{a}(\chi^2 - 1)\right)^{1/2} \quad (4)$$

with

$$\chi = \exp\left(\frac{\pi E_0 v_c}{8 p_c a}\right) \quad (5)$$

Now with the DBCS representation of a cohesive zone, the fracture toughness, K_{Ic}, associated with crack extension under linear elastic fracture mechanics conditions, i.e. where the cohesive zone is small compared with all the geometrical parameters associated with a configuration, is given by the relation

$$K_{Ic} = (E_0 p_c v_c)^{1/2} \quad (6)$$

whereupon Equations 3 and 5 can be written as

$$\frac{\sigma_{eff}}{p_c} = 1 + \frac{2}{\pi}\left(\frac{a}{p}\right)^{1/2} \sec^{-1}\left[\exp\left(\frac{\pi K_{Ic}^2}{8 p_c^2 a}\right)\right] \quad (7)$$

and

$$\chi = \exp\left(\frac{\pi K_{Ic}^2}{8 p_c^2 a}\right) \quad (8)$$

respectively. When $\pi K_{Ic}^2/8 p_c^2 a \equiv \theta$ is less than 0.7,

$$\sec^{-1}\left[\exp\left(\frac{\pi K_{Ic}^2}{8 p_c^2 a}\right)\right] \equiv \sec^{-1}[\exp(\theta)] = (2\theta)^{1/2} \quad (9)$$

to within an accuracy of about 10%. Moreover, again for small θ, Equation 4 simplifies to

$$\frac{s}{a} = \left(\frac{2\rho\theta}{a}\right)^{1/2} + \theta \quad (10)$$

or

$$\frac{s}{\rho} = \left(\frac{2a\theta}{\rho}\right)^{1/2} + \frac{a\theta}{\rho} \quad (11)$$

Thus, provided that $\pi K_{Ic}^2/8 p_c^2 a$ is small, i.e. less than 0.7 (see comment preceding Equation 9), Equations 7 and 9 give

$$\frac{\sigma_{eff}}{p_c} = 1 + \frac{K_{Ic}}{p_c(\pi\rho)^{1/2}} \quad (12)$$

Furthermore, provided that ρ is not small compared with a, Equations 10 and 11 show that both s/a and s/ρ are small. Vice versa, if both s/a and s/ρ are small, θ is small and Equation 12 is appropriate.

Interestingly, and most importantly, the preceding analysis shows that it is the hole root radius ρ which is the hole geometry length parameter that enters into

the simplified expression in Equation 12 for the effective failure stress, σ_{eff}. With the mode III semi-elliptical hole model used in this section, the root radius ρ characterizes the elastic stress gradient immediately ahead of the hole tip, i.e. if $\sigma(x)$ is the appropriate stress at a distance x from the hole root surface and σ_L is the stress at the surface, then [8]

$$\sigma(x) = \sigma_L\left(1 - \frac{x}{\rho}\right) \tag{13}$$

for small x. That being the case, it is reasonable to suggest that, with a general hole not necessarily semi-elliptical and not necessarily with mode III loading, if the elastic stress immediately ahead of the hole is of the form given by Equation 13 but with ρ replaced by a more general parameter h, then there should be a simple effective failure stress relation similar to Equation 12, but with ρ replaced by h. The analyses in the next two sections provide support for this assertion.

4. The planar surface simulation procedure: mode III analysis

Consider the mode I situation where there is a cohesive zone emanating from a planar surface of a semi-infinite solid (Fig. 2). It is assumed that the tensile stress along the plane $X_2 = 0$ in the absence of the cohesive zone is

$$\sigma(x) = \sigma_L\left(1 - \frac{x}{h}\right) = K_t\sigma\left(1 - \frac{x}{h}\right) \tag{14}$$

where x is measured from $X_1 = 0$ along the X_I axis. This stress simulates the tensile stress ahead of the root of a hole where σ is the applied stress, K_t is the elastic stress concentration factor, σ_L is the stress at the flaw surface and h is a length parameter.

In line with the earlier considerations in this paper, and with p_c being the (constant) tensile stress within the cohesive zone, the maximum-stress situation is assumed to be attained when the relative displacement within the cohesive zone attains a critical value, v_c. For the corresponding mode III situation, isolated-crack–infinite-body solutions can be used, by making a cut along the plane $X_1 = 0$. Applying these solutions to the mode I loading state, the condition for stress finiteness (equal to p_c) at the leading edge of the process zone is

$$\frac{\pi}{2}(\sigma_L - p_c) - \frac{\sigma_L s}{h} = 0 \tag{15}$$

while the relative displacement condition at $x = 0$ is

$$v_c = \frac{4s(\sigma_L - p_c)}{E_0} - \frac{4s^2\sigma_L}{\pi E_0 h} \tag{16}$$

Now $\sigma_L = \sigma_{eff}$, the effective failure stress appropriate for use in a traditional elastic stress analysis, whereupon elimination of s between Equations 15 and 16 gives

$$\frac{\sigma_{eff}}{p_c} = 1 + \psi\left(1 + \frac{\psi^2}{4}\right)^{1/2} + \frac{\psi^2}{2} \tag{17}$$

with $\psi = K_{Ic}/p_c(\pi h)^{1/2}$ assuming, as before, that $K_{Ic} = (E_0 p_c v_c)^{1/2}$. The right-hand side of Equation 17 can be expanded in terms of increasing powers of ψ when, to the second term, it becomes

$$\frac{\sigma_{eff}}{p_c} = 1 + \frac{K_{Ic}}{p_c(\pi h)^{1/2}} = 1 + \frac{0.56K_{Ic}}{p_c h^{1/2}} \tag{18}$$

Now, as regards the geometrical parameter h that characterizes the stress distribution ahead of the surface of an actual hole, with the mode III model of a semi-elliptical hole in a uniformly stressed infinite solid, h is equal to ρ, the hole root radius (see Equation 13). In this case, Equation 18 is identical with Equation 12. This equivalence demonstrates very clearly the potential for using the planar surface simulation procedure coupled with a linear "applied" stress distribution, in lieu of a detailed cohesive zone analysis for an actual hole, expecting this approach to be reasonably accurate provided that the cohesive zone size is small compared with both the hole size and the root radius. In the next section we derive an expression for the effective failure stress on the basis of actual mode I results from a planar surface analysis.

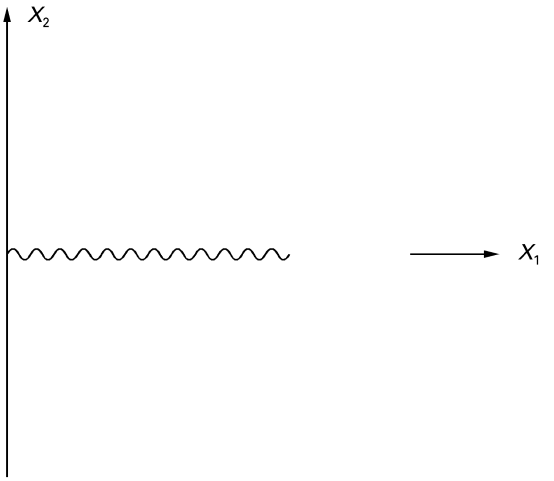

Figure 2 The planar surface model analyzed in Section 4.

5. The planar surface simulation procedure: mode I analysis

In this section, the objective is to obtain a relation of the form of Equation 18, using actual mode I results rather than making use of mode III results, as was the case in the preceding section. The quoted results of Tada *et al.* [9] show that the condition for stress finiteness at the leading edge of the process zone (see Fig. 2) is

$$1.12(\sigma_L - p_c) - \frac{2.14\sigma_L s}{\pi h} = 0 \tag{19}$$

while the relative displacement condition at $x = 0$ is

$$v_c = \frac{5.83s(\sigma_L - p_c)}{E_0} - \frac{1.77s^2\sigma_L}{E_0 h} \tag{20}$$

these relations being analogous to Equations 15 and 16, respectively, for the mode III analysis. With $\sigma_L = \sigma_{eff}$, the effective failure stress, elimination of s between Equations 19 and 20 gives, to the first term in powers of $K_{Ic}/p_c h^{1/2}$ and again with $K_{Ic} = (E_0 p_c v_c)^{1/2}$,

$$\frac{\sigma_{eff}}{p_c} = 1 + \frac{0.46K_{Ic}}{p_c h^{1/2}} \tag{21}$$

a relation which is analogous to Equation 18 obtained from a mode III analysis. We immediately see that there is a close correspondence between the two sets of results.

As an example of an application of the mode I Equation 21, consider the elliptically cylindrical hole model shown in Fig. 1. In this case a detailed analysis (see the Appendix) shows that the parameter h describing the stress distribution (see Equation 14) ahead of the hole (mode I loading) is given by the expression

$$h = \frac{\rho}{2}\left[1 + \frac{1}{2}\left(\frac{\rho}{a}\right)^{1/2}\right] \Big/ \left[1 + \frac{3}{4}\left(\frac{\rho}{a}\right)^{1/2}\right] \tag{22}$$

whereupon $h \approx \rho/2$ for a wide range of hole profiles, showing that it is the hole root radius that is the geometry parameter that governs the magnitude of the effective failure stress (see Equation 21). Equation 22 checks with the well-known solution [10] for a circular hole ($\rho = a$) when $h = 3a/7$. Equations 21 and 22 allow the effective failure stress to be given by the relation

$$\frac{\sigma_{eff}}{p_c} = 1 + \frac{0.67K_{Ic}}{p_c \rho^{1/2}} \tag{23}$$

where the second term on the right-hand side of this relation is accurate to within 2% for a/ρ lying within [11] the range $1 \to 5$. Now Vitek [11] has undertaken a numerical analysis of the mode I model in Fig. 1, based on the representation of the displacement discontinuity within the cohesive zones in terms of discrete dislocations, and the reduction of the problem to the solution of a system of linear equations. When $K_{Ic}/p_c a^{1/2}$ is small (this condition is implicit in the considerations leading to Equation 18), Vitek's curve-fitted results can be reframed so as to give the following expression for the effective failure stress:

$$\frac{\sigma_{eff}}{p_c} = 1 + \frac{K_{Ic}}{p_c(\pi\rho)^{1/2}} \frac{1}{\frac{1}{2} + (\rho/a)^{1/2}/[1 + \frac{1}{2}(\rho/a)^{1/2}]^3} \tag{24}$$

simplifying to

$$\frac{\sigma_{eff}}{p_c} = 1 + \frac{0.73K_{Ic}}{p_c \rho^{1/2}} \tag{25}$$

where the second term on the right-hand side of this relation is accurate to within 3% for a/ρ lying within the range $1 \to 5$. There is good agreement between Equations 23 and 25. Such an agreement for mode I loading coupled with the similar agreement for mode III loading provides confidence in using the elastic stress gradient h ahead of a hole as input towards estimating the effective failure stress, the appropriate relation (mode I) giving σ_{eff} being Equation 21.

6. Concluding comments

The paper has been concerned with the geometry dependence of the effective failure stress of an uncracked brittle structure, proceeding from the basis that it is related to the formation of a damage zone at a free surface. The damage is represented by a cohesive zone, and the maximum load (i.e. failure) is associated with the attainment of an elastically calculated effective tensile failure stress. The paper has been specifically concerned with the effective stress associated with the formation of a damage zone at the surface of a blunt stress concentration and it has been shown that the key parameter that affects the magnitude of this stress is the stress gradient ahead of the stress concentration, and this is related to the root radius of the concentration.

Appendix

Fig. 1 shows the two-dimensional model of an elliptically cylindrical flaw in an infinite solid that is subjected to a tensile stress, σ, normal to the major axis of the flaw; the semiminor and semimajor axes are of lengths b and a, respectively. The objective of the analysis in this Appendix is to determine the stress p_{22} along the X_1 axis ahead of the right-hand flaw root to the first two terms in the expansion of this stress, i.e. the parameter h in the expansion

$$p_{22} = K_t \sigma \left(1 - \frac{x}{h}\right) \tag{A1}$$

where $K_t = 1 + 2(a/\rho)^{1/2}$, with x being measured along the X_1 axis away from the flaw root.

The standard solution giving the elastic stress distribution in the solid can be described by the expressions [12]

$$p_{11} + p_{22} = 2[\phi'(z) + \bar{\phi}'(\bar{z})] = 4R[\phi'(z)] \tag{A2}$$

$$p_{22} - p_{11} + 2ip_{12} = 2[\bar{z}\phi''(z) + \chi''(z)] \tag{A3}$$

where $z = X_1 + iX_2$, and with the usual complex variable terminology. Based on the transformation

$$z = \beta \cosh \psi \tag{A4}$$

where $a = \beta \cosh \psi_0$ and $b = \beta \sinh \psi_0$, the functions ϕ and χ in Equations A2 and A3 are given by the expressions

$$\phi(z) = A \cosh \psi + B \sinh \psi \tag{A5}$$

$$\chi(z) = D\psi + E \cosh[2(\psi - \psi_*)] \tag{A6}$$

where A, B, C, D and ψ_* are given by the relations

$$A = -\frac{\beta\sigma}{4}\exp(2\psi_0)$$

$$B = \frac{\beta\sigma}{4}[1 + \exp(2\psi_0)]$$

$$D = -\frac{\beta^2\sigma}{4}[1 + \cosh(2\psi_0)] \quad \text{(A7)}$$

$$E = -\frac{\beta^2\sigma}{8}\exp(2\psi_0)$$

$$\psi_* = \psi_0 + \frac{i\pi}{2}$$

It follows from Equations A2–A7 that, along the X_1 axis ahead of the flaw root, the expression for p_{22} is

$$p_{22} = \frac{2}{\beta}(A + B\coth\psi) - \frac{X_1 B}{\beta^2\sinh^3\psi} - \frac{D\cosh\psi}{\beta^2\sinh^3\psi} + \frac{2E}{\beta^2\sinh^2\psi}\left(\frac{\sinh[2(\psi-\psi_0)]\cosh\psi}{\sinh\psi} - 2\cosh[2(\psi-\psi_0)]\right) \quad \text{(A8)}$$

with ψ being real. With $\psi = \psi_0 + \Delta\psi$ and $X_1 = a + x$, where $\Delta\psi$ and x are both presumed to be small, it follows that, to the first term in x, we have

$$p_{22} = \sigma\left(1 + \frac{2a}{b}\right) \quad \text{(A9)}$$

this being, of course, the standard elastic stress concentration result. As regards the second term, it follows from Equation A8 that

$$\frac{4p_{22}b}{\sigma x} = \frac{3}{\sinh^4\psi_0}[1 + (\cosh\psi_0 + \sinh\psi_0)^2] + \frac{2\cosh^3\psi_0}{\sinh^3\psi_0}(\tanh\psi_0 - 3\coth\psi_0) - \frac{6\cosh\psi_0}{\sinh^3\psi_0}(\cosh\psi_0 + \sinh\psi_0)^2 \quad \text{(A10)}$$

which simplifies to

$$p_{22} = -\frac{\sigma x\cosh\psi_0(4\cosh\psi_0 + 3\sinh\psi_0)}{a\sinh^2\psi_0} \quad \text{(A11)}$$

It then follows by reference to Equation A1, and with $K_t = 1 + 2(a/b) \equiv 1 + 2(a/\rho)^{1/2}$, that the parameter h is given by the relation

$$h = \frac{K_t b\sinh^2\psi_0}{\cosh\psi_0(4\cosh\psi_0 + 3\sinh\psi_0)} \quad \text{(A12)}$$

or, with $a = \beta\cosh\psi_0$ and $b = \beta\sinh\psi_0$,

$$h = \frac{K_t b^3}{a(4a + 3b)} \quad \text{(A13)}$$

Expressed in terms of the flaw root radius, this relation becomes

$$h = \frac{\rho}{2}\frac{1 + \frac{1}{2}(\rho/a)^{1/2}}{1 + \frac{3}{4}(\rho/a)^{1/2}} \quad \text{(A14)}$$

References

1. J. OZBOLT and R. ELIGEHAUSEN, in "Size-scale effects in the failure mechanisms of materials and structures", edited by A. Carpinteri (E. & F. N. Spon, London, 1996) p. 290.
2. M. ELICES, G. V. GUINEA and J. PLANAS, *ibid.* p. 309.
3. Y. N. LI and Z. P. BAZANT, *ibid.* p. 274.
4. E. SMITH , *J. Mater. Sci.* (1997), in press.
5. D. S. DUGDALE, *J. Mech. Phys. Solids* **8** (1960) 100.
6. B. A. BILBY, A. H. COTTRELL and K. H. SWINDEN, *Proc. Roy. Soc. A*, **272** (1963) 304.
7. E. SMITH, *ibid. A* **299** (1967) 455.
8. *Idem., Int. J. Engng Sci.* **6** (1968) 129.
9. H. TADA, P. C. PARIS and G. R. IRWIN, "The stress analysis of cracks handbook" (Del Research Corporation, Hellertown, PA, 1973).
10. J. F. KNOTT, "Fundamentals of fracture mechanics" (Butterworth, London, 1973).
11. V. VITEK, *J. Mech. Phys. Solids*, **24** (1976) 67.
12. J. C. JAEGER, "Elasticity, fracture and flow" (Methuen, London, 1969).

Received 9 June
and accepted 29 July 1997